Density and refractive index of thin evaporated films

Dieter Mergel[1*] and Martin Jerman[2]

[1] *Physics Department, University of Duisburg-Essen, 47048 Duisburg, Germany*

[2] *Optical Workshop, University of Duisburg-Essen, 45117 Essen, Germany*

[*] *E-mail: dieter.mergel@uni-due.de*

Received October 26, 2009

Optical coatings based on multilayers are prepared. The dependence of the refractive index of SiO_2, TiO_2, HfO_2, and ZrO_2 on the conditions during thin film evaporation (e.g., oxygen partial pressure, substrate temperature) and upon post-annealing are investigated in detail. For coatings to be stable under intensive laser irradiation, post-heating of the evaporated films is necessary. The correlation between mass density and refractive index is analysed on the basis of a model comprising compact grains (i.e., amorphous or crystalline) and pores filled with air or water. The properties of the whole film are discussed on the basis of an effective-medium model, whereas the properties of a single grain are derived from a general refractivity formula valid for homogeneously distributed dipoles.

OCIS codes: 310.0310, 310.1860, 310.3840, 310.6860.

doi: 10.3788/COL201008Sl.0067.

In the optical workshop of the University of Duisburg-Essen, customized optical coatings for laser applications are designed and produced. To design multilayer coatings according to predefined optical spectral characteristics, precise dispersion curves in the relevant spectral range of the thin film materials involved have to be known.

The films were deposited by electron-beam evaporation in a Balzers BAK-640 high-vacuum chamber. Circular glass substrates (Schott B270, 1-mm thick with a diameter of 25 mm) and quartz substrates (Schott Lithosil Q1, 2-mm thick, 25-mm diameter) were used. The substrate temperature was 300 °C for most of the depositions. The thickness of the films ranged from 0.15 to 1.5 μm. The base pressure before deposition was 3×10^{-4} Pa. For a robust production process, the background pressure must not be too low because it does not yield a reproducible oxygen partial pressure. Therefore, the oxygen partial pressure during deposition was varied from 1 to 8×10^{-2} Pa.

In the course of our experiments, it was found that it is important to determine the mass density of the films and its relation with the refractive index. Simple analytical methods will be described in detail. The methods were checked on a variety of materials (e.g., MgF, SiO_2, Al_2O_3, ZrO_2, HfO_2, and TiO_2) with refractive indices n ranging from 1.35 to 2.5 and film thicknesses d ranging from 150 to 1500 nm. The relationship between the oxygen pressure during deposition, the packing density, and the refractive index of the films was investigated in detail for TiO_2[1,2], SiO_2[3,4], HfO_2[3], and ZrO_2[3], which are hard, durable, and laser-damage resistant materials of low or high refractive index. They are widely used to realise multilayered coatings, also in the ultraviolet (UV) spectral range.

In the literature, the relationship between refractive index and mass density is described as linear. Such relationship is also valid for our experimental results. However, this study goes one step further and attempts to deduce the mass density and the refractive index of a single grain in the films from such a relationship. As will be seen, the results can only be obtained by making hypotheses on the microstructure of the films and on the structure of a single grain.

The mass of the films is determined by weighing the substrates before and after coating and taking the difference of the two measurements. This is a critical procedure because the film mass is much lower than the substrate mass and is prone to many errors. To obtain reliable results, it is useful to simultaneously coat at least two substrates in the same deposition process. The difference between the two masses is an indication of the statistical measurement error.

There exist various possibilities to determine the thickness of a film. One is to deduce the thickness from interference fringes in the transmittance or reflectance or ellipsometric spectra[5,6]. In this case, the refractive index at the positions of the extrema of the spectra has to be known. The corresponding procedure will be described later. Also, for the film thickness, it is important to perform several measurements with different methods in order to estimate their reliability and the statistical error.

Another possibility is to determine the film thickness with a profilometer. When the substrate is coated from below with the particle source, there is usually an uncoated fringe due to the substrate holder. Determination of the thickness is then most easily done at the edge of the substrate. However, one must be aware that shadowing effects exist, which tend to round the edge of the film near the mask. This should be carefully measured by extending the lateral profilometer range. In our workshop, we often follow another procedure to at least check the reliability of the measurement at the edge. The substrate is firstly marked by using a felt pen. The film on top of this mark is easily removed by rubbing, yielding a sharp edge at which the film thickness is more reliably determined.

An efficient method to evaluate the optical spectra is through dielectric modelling. The theoretical spectra are calculated by dielectric modelling, and the experimental data are fitted by varying the parameters of the model. A commercial software program[7] is used in this study, which has already been successfully applied to In_2O_3:Sn[8] and ZnO:Al[9] films. The model for

electrically isolating films investigated in this study is comprised of a single harmonic oscillator to account for interband transitions and a term representing the optical transitions close to the band edge. For the degenerate semiconductor In_2O_3:Sn, a third term that considers intraband transitions due to free electrons had to be added but is not needed here. The method used in the current study also has the advantage of taking absorption into account; for example, a value for the band gap is returned.

The refractive index of a thin completely transparent film can be determined from the minimum transmittance of the coated substrate, T_c, when the index of the film is higher than that of the substrate. In this case, the maxima of the transmittance spectrum are equal to the transmittance of the uncoated substrate. When the index of a film is lower than that of the substrate, as in the case of SiO_2 films, the maximum transmittance has to be taken. In any case, the second parameter that has to be determined experimentally is the transmittance of the uncoated substrate, T_0, at the wavelength of the extremum under consideration.

The reflectance of the coated substrate from the measured transmittances T_c and T_0 can be calculated by using

$$R_c = \frac{2T_0 - T_c\,(T_0 + 1)}{2T_0 + T_c\,(T_0 - 1)}. \tag{1}$$

Substituting the calculated entity into Eq. (1) for the refractive index of the coating, n_2, yields the following:

$$n_2 = \sqrt{n_1 n_3 \frac{1 + \sqrt{R_c}}{1 - \sqrt{R_c}}}, \tag{2}$$

where n_1 and n_3 are the refractive indices of the substrate and air, respectively[5,6].

The packing density of the evaporated films is shown in Fig. 1 for four materials (i.e., TiO_2, SiO_2, ZrO_2, and HfO_2) as a function of pressure during deposition. The curves fit the experimental data in Refs. [1] and [3].

Generally, a decrease in density with an increase in pressure is observed. This was correlated with the decrease in free path in the chamber, which was estimated

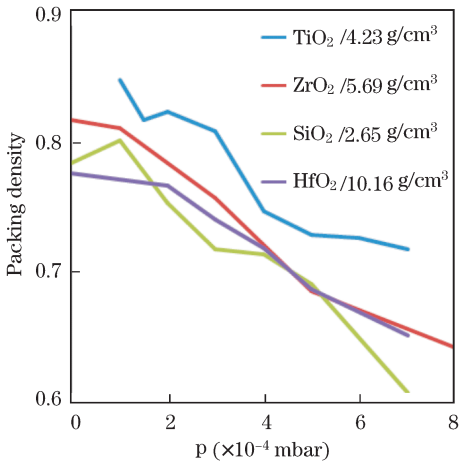

Fig. 1. Packing density of evaporated films. The density of the crystalline materials used as a reference is given in the legend.

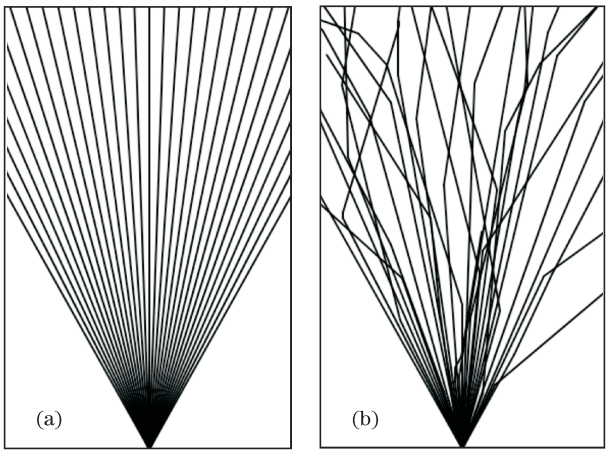

Fig. 2. Path of the evaporated species under (a) low pressure and (b) high pressure.

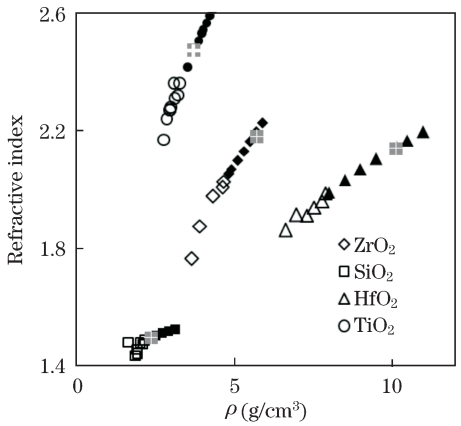

Fig. 3. Refractive index as a function of the density. Experimental results (open symbols) and theoretical values of hypothetical compact grains.

by the well-known formula from the kinetic theory of gases[10]:

$$\lambda = \frac{RT}{\sqrt{2} N_A \sigma p}, \tag{3}$$

where N_A is the Avogradro's constant, σ is the collison cross section of the gas species, p is the pressure. With an estimated value of the crucible temperature of 1250 K, the mean free path in Eq. (3) becomes 75 cm, which is the distance between the crucible and the substrate, for a pressure of 3.5×10^{-4} mbar. Therefore, the decrease in packing density of the evaporated films is due to the thermalization of evaporated species; the main effect is that the particles do not reach the growing film from a unique angle but chaotically from all sides. This situation is depicted in Fig. 2(b).

For TiO_2, there is an additional effect. The films deposited at 1×10^{-4} mbar are black, thus indicating a sub-oxidic phase with higher mass density.

The refractive index of the evaporated thin films as a function of film density for the coating materials TiO_2, SiO_2, HfO_2, and ZrO_2 has been determined. The results of the last three materials together with the results from the literature for TiO_2 are summarized in Fig. 3 using open symbols. The closed symbols represent the potential values of hypothetical compact grains that form, to-

gether with the pores, the packing of the thin films.

The most important basic microscopic entity determining the complex refractive index, that is, the real refractive index and the extinction coefficient, is a harmonic oscillator, which is described by the parameters' position on the energy (or wavelength) scale, strength, and damping constant. This is an ideal entity. Real matter is described by a spectrum of harmonic oscillators, that is, the density of harmonic oscillators on the energy (frequency) scale. This density in frequency space is determined by the density in real space, that is, the more oscillators there are in a unit volume, the higher is the accumulated strength of the oscillators at the corresponding eigen frequency. This theory is the basis of numerous works that relate the refractive index and mass density of thin films[11−15].

There are additional parameters that determine the density in frequency space. The most important one is the energetic position of the harmonic oscillator. However, the parameter is different for an amorphous and crystalline material, and this has to be taken into account when a film is a mixture of the amorphous and crystalline phases. Another complication arises for TiO_2 with two crystalline phases, anatase and rutile, which have different band gaps. As a result, there are different indices of refraction in the whole visible wavelength region. This is a well-known fact but is often ignored in the theoretical analysis of optical data.

This is important for practical reasons. The effects of depositing temperature on the structural and optical properties of a TiO_2 film have been investigated in Ref. [16] with preparing the films by ion beam-assisted electron-beam deposition. The as-deposited films were all amorphous. After annealing at 450 °C for 1 h in vacuum, the samples showed small crystalline peaks of anatase. The highest transparency over the visible wavelength region was obtained for the highest deposition temperature of 300 °C. The annealed films exhibited a refractive index of 2.29 at a wavelength of 550 nm.

Point defects in crystalline or amorphous materials introduce additional absorption centers that may usually also be described by harmonic oscillators. These change the refractive index of the film. Usually, the refractive index becomes higher in the visible and infrared range because the energy of the defects is often close to the band edges and introduces optical transitions just below the fundamental transition across the band gap.

The macroscopic parameters, density ρ and index of refraction n, of thin films are often related to one another by a Lorentz-Lorenz plot based on the Clausius-Mossotti relation[17,18]:

$$\frac{\varepsilon-1}{\varepsilon+2}=\frac{4\pi}{3}N\alpha_{\mathrm{m}}(cgs), \tag{4}$$

where N is the concentration, and α_{m} is the polarisability of a point-like "molecule." This equation is applicable only in cases where the dipoles are distributed homogeneously in space as schematically shown in Fig. 4.

Treating the atoms as ideal point dipoles is not valid for compounds with covalent bonding. This is considered

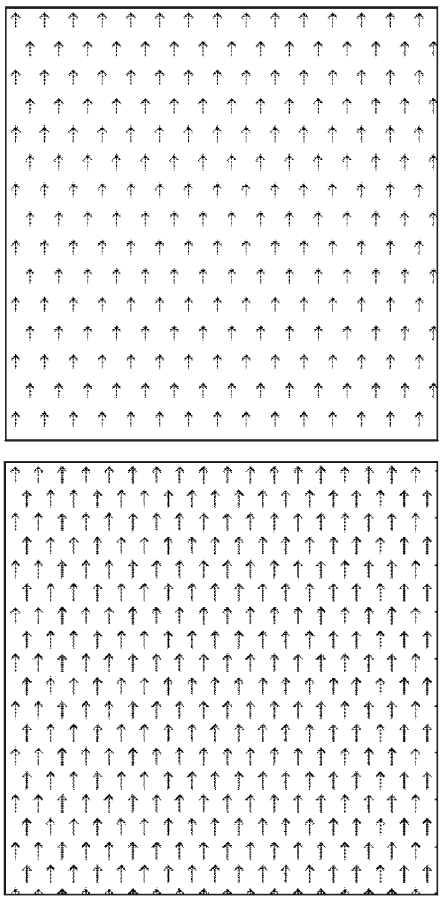

Fig. 4. Homogeneous distribution of point dipoles with various densities. Situation for which the Lorentz-Lorenz formula and the general refractivity formula are valid.

by a more general refractivity formula[19]

$$\frac{n^2-1}{4\pi+b(n^2-1)}=\frac{\alpha}{M}\rho, \tag{5}$$

where (α/M) is the polarisability divided by the molecular weight M. The local electric field is

$$\boldsymbol{E}_{loc}=\boldsymbol{E}+b\boldsymbol{P}, \tag{6}$$

where b comprises the effects of the depolarisation field $4\pi\boldsymbol{P}/3$ and an overlap field $\gamma\boldsymbol{P}$: $b=4\pi/3–\gamma$. The Lorentz-Lorenz relation in Eq. (4) becomes Eq. (5) for $\gamma=0$, which results in $b=4\pi/3$. As mentioned above, this is valid for the case of point dipoles (i.e., no overlap of neighbouring orbitals) at a cubic eighbourhood.

To describe the (n, ρ) data of various isochemical series of densified silica glasses, Eq. (5) was used[19]. Another group of researchs synthesized various glasses with direct, sol-gel, or vapour-phase axial deposition and established linear relationships between the refractive index and the density based on the general refractivity formula[20].

This formula is also useful in discussing the refractive index in mixed oxides. Ferrer *et al.* studied the connection between the optical properties and electronic parameters derived from an X-ray photoelectron spectrometer (XPS) analysis of materials with mixed oxides (e.g., SiO_2-TiO_2 and SiO_2-ZrO_2 thin films)[21]. They

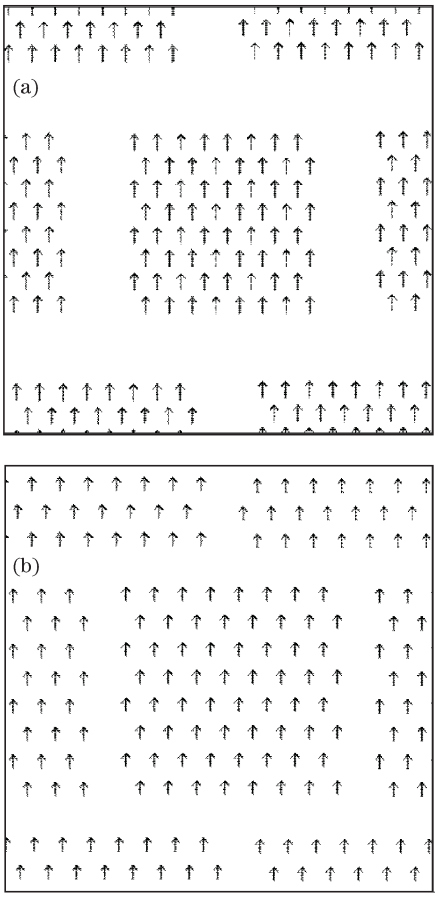

Fig. 5. Model for the microstructure of a thin film consisting of compact grains and pores. The single grain in (a) exhibits higher density and higher refractive index than the grain in. The porosity in (a) is larger. The density and the refractive index of the complete film are the same.

Table 1. Density and Refractive Index of Some Crystalline Phases.

Material	ρ(g/cm^3)	n	λ(nm)	Ref.
SiO_2				
Fused Quartz	2.2	1.460	546	3
Crystal Quartz	2.653	1.546, 1.555	546	3
	2.65	1.544, 1.553	589	3
Cristobalite	2.32	1.487, 1.484	589.3	3
TiO_2				
Anatase	3.84	2.59, 2.52	546	25
Rutile	4.23	2.65, 2.95	546	25
Brookite	4.12			26
ZrO_2				
Monoclinic	5.68	2.176	?	3
Basseleyite	5.7	2.13, 2.19,2.20	?	3
HfO_2				
Monoclinic	10.14	?		3
Cubic	?	2.125	550	3

analyzed their results using the general refractivity formula and assumed that the various polarizabilities add according to the volume density of the corresponding centers.

Another interesting result of the refractivity formula is discussed by He *et al.*[22], where Lorentz-Lorenz simplification was used. The authors assumed that the refractive index is related to the density and polarizability of a given material by the Lorentz-Lorenz relation. The variation in the refractive index could be caused by changes in density and/or polarizability. The authors also concluded that incorporation of nitrogen increases the refractive index because the metal-nitrogen bonds tend to be less polar than the corresponding metal-oxygen bonds, thus leading to a higher polarizability for the metal nitrides.

The Brüggeman effective medium approach was applied to the thin films presented above in Fig. 3. The approach yields the dielectric constant ε' and the density ρ of a mixture of two phases with dielectric constants ε_1 (volume fraction q_1) and ε_2 (volume fraction $1-q_1$) and densities ρ_1 and ρ_2. The relevant formula is shown below[23]

$$q_1\left(\frac{\varepsilon'-\varepsilon_1}{\varepsilon'+2\varepsilon_1}\right)+(1-q_1)\left(\frac{\varepsilon'-\varepsilon_2}{\varepsilon'+2\varepsilon_2}\right)=0, \tag{7a}$$

$$\rho=q_1\rho_1+(1-q_1)\rho_2. \tag{7b}$$

The quotients in Eq. (7a) describe the depolarizing fields of single grains of the two phases embedded in a homogeneous medium with a hypothetical effective macroscopic dielectric constant ε'. The left-hand side of Eq. (7a) represents the average depolarizing field. The value of ε' is determined by the condition that the field is zero.

The underlying assumption of the model in this study is that the films consist of compact grains and pores. As the pore volume is not known from independent measurements, it is indirectly deduced. This was done by initially assuming that the compact grains in the films have a certain mass density, which is the same for the whole series of evaporated films under investigation. The refractive index was then deduced from this hypothetical grain that best explains the experimental refractive indices and mass densities of the films. Each choice of density led to a different refractive index of the compact grain as visualized in Fig. 5.

For different hypothetical grain mass densities, different values of the refractive index were obtained. The corresponding data points are represented in Fig. 3 by full symbols.

It should also be mentioned that the porosity of thin films can be measured directly. The open porosity of the thin TiO_2 films was determined by measuring water absorption-desorption isotherms with a quartz crystal monitor[24]. For samples prepared with mixtures of $Ar+O_2$, the constituents of porosity were based from micropores ($d < 2$ nm), whereas the films prepared with a pure oxygen plasma contained mesopores ($d > 2$ nm).

Among a number of possible parameters of compact grains, physically meaningful ones have to be chosen. The second hypothesis was thus proposed: the compact grains exhibit an expanded crystalline structure. In this case, the general refractivity formula, or in special

cases, the Lorentz-Lorenz formula, is valid because the material is homogeneous. This phenomenon is shown in Fig. 4. The properties of crystalline grains sourced from the literature are summarized in Table 1. The atomic arrangement of amorphous TiO_2 has been found to resemble that of brookite and can be described as an assembly of short staggered chains of Ti-O octahedral[27].

For the various materials, the relationship $n = n(\rho)$ is calculated on the basis of the general refractivity formula. The cross-section of this curve with the line for the hypothetical grains that explain the data points is indicated in Fig. 3 with the white crosses in a grey square.

The compact grains satisfying the two hypotheses have the following properties. For ZrO_2, the density was about 5.7 g/cm^3, and the refractive index was 2.17. These values correspond to the values for the crystalline phase of baddeleyite. For HfO_2, the density was about 9.7 g/cm^3 which was in the refractive index range of 9.7−10.14 reported for the monoclinic crystalline phase. For SiO_2, the density was 2.36 g/cm^3, which is a little higher than that of crystobalite (2.32 g/cm^3) and 7% higher than that of fused quartz. For TiO_2, the density was 0.97 that of anatase (3.84 g/cm^3).

The above estimation of the density of an amorphous grain has been used in molecular dynamics simulation done for a spherical particle (with the "real" density of 3.8 g/cm^3) for amorphous TiO_2[28].

The established relationship also enables the estimation of the refractive index when the pore volume is known from measurements. Scanning electron microscopy images indicated that the sample had a porosity of 15%. Thus, the refractive index was accordingly reduced by this volume[29].

The refractive index of SiO_2 films deposited by electron beam evaporation at 300 °C decreases upon post-heating[4]. This is explained by the annealing of point defects that introduce electron states close to the band edges.

Similar effects have been observed in other studies, e.q., in a comparison of films prepared by the sol-gel technique. The films deposited by the sol-gel technique are amorphous and exhibited a lower refractive index than the evaporated films, which is attributed to less absorption due to a smaller defect density[30]. The evaporated films were deposited at 300 °C and annealed at 400 °C; they showed crystalline peaks in the XRD (X-ray diffraction) image. Thus, the relationship between packing density and refractive index of the films is obtained on the basis of Bruggeman effective-medium approximation.

Further, defect density depends on the deposition rate. This was evidenced by the laser damage threshold of the TiO_2/SiO_2 high reflectors[31]. The refractive index increased with the rate of deposition. The absorption is the lowest, and the damage threshold is the highest for the lowest deposition rate.

In conclusion, the mass density of TiO_2, SiO_2, HfO_2, and ZrO_2 is found to be a function of the pressure during deposition. The packing density with respect to the crystalline phases decreases in all cases with increasing pressure. This is attributed to increased scattering of the particle beam in the evaporation chamber, which led to chaotically directed particles deposited at the growing film.

The refractive index is often a linear function of the density. However, it does not follow the Clausius-Mosotti relation. This is most evident in the Lorentz-Lorenz plots that yield a non-zero ordinate intercept, which is contrary to theory. The reason is that the varying density is not due to homogeneously distributed oscillators but various pore volumes.

An analysis of the data for ρ and n on the basis of the Bruggeman effective medium approach allows the estimation of the density and refractive index of a single compact grain in a porous film structure. The underlying model assumes that in a series of films with various mass densities, the compact grains are always the same, and only the pore volume changes. This is certainly questionable, and more sophisticated models should be tested.

The refractive index is also determined by other structural parameters aside from mass density. In the case of TiO_2, the coexistence of various phases with different ρ and n (i.e., amorphous, anatase, and rutile) has to be taken into account. For SiO_2, it can be concluded from the data that during fast deposition, a certain amount of point defects is introduced into the thin film, which gives rise to energy levels close to the band edges. This introduces extra absorption close to the fundamental interband absorption and increases the refractive index in the visible spectral range due to the Kramers-Kronig relation. Upon post-heating, the defects disappear, and the refractive index decreases. Therefore, the density of a thin film of a certain material alone does not determine the refractive index.

References

1. D. Mergel, D. Buschendorf, S. Eggert, R. Grammes, and B. Samset, Thin Solid Films **371,** 218 (2000).
2. M. Jerman and D. Mergel, Thin Solid Films **515,** 6904 (2007).
3. M. Jerman, Z. Qiao, and D. Mergel, Appl. Opt. **44,** 3006 (2005).
4. M. Jerman and D. Mergel, Thin Solid Films **516,** 8749 (2008).
5. R. Swanepoel, J. Phys. E. Sci. Instrum. **16,** 1214 (1983).
6. H. Ahrens, "Bestimmung der Absorptionsindices und der Struktur dielektrischer Aufdampfschichten in Abhängigkeit von den Herstellungsparametern", PhD. Thesis (Technische Universität Hannover, 1974).
7. B. Klein, "Hard-and Software for Optical Spectroscopy", http://www.mtheiss.com (February 17, 1998).
8. D. Mergel and Z. Qiao, J. Phys. D: Appl. Phys. **35,** 794 (2002).
9. Z. Qiao, C. Agashe, and D. Mergel, Thin Solid Films **496,** 520 (2006).
10. P. W. Atkins, *The Elements of Physical Chemistry* (Oxford University Press, Oxford, 1975).
11. C. R. Ottermann and K. Bange, Thin Solid Films **286,** 32 (1996).
12. H. K. Pulker, G. Paesold, and E. Ritter, Appl. Opt. **15,** 2986 (1976).
13. E. E. Khawaja, F. Bouamrane, F. Al-Adel, A. B. Hallak, M. A. Daous, and M. A. Salim, Thin Solid Films **240,** 121 (1994).
14. M. Laube, R. Rauch, C. Ottermann, O. Anderson, and

K. Bange, Nucl. Instrum. Meth. Phys. Res. B **113,** 288 (1996).
15. J. M. Bennett, E. Pelletier, G. Albrand, J. P. Borgogno, B. Lazarides, C. K. Carniglia, R. A. Schmell, T. H. Allen, T. Tuttle-Hart, K. H. Guenther, and A. Saxer, Appl. Opt. **28,** 3303 (1989).
16. C. Yang, H. Fan, Y. Xi, J. Chen, and Z. Li, Appl. Surf. Sci. **254,** 2685 (2008).
17. D. E. Aspnes, Am. J. Phys. **50,** 704 (1982).
18. D. E. Aspnes, Thin Solid Films **89,** 249 (1982).
19. J. Arndt and W. Hummel, Phys. Chem. Minerals **15,** 363 (1988).
20. N. Kitamura, K. Fukumi, J. Nishii, and N. Ohno, J. Appl. Phys. **101,** 123533 (2007).
21. F. J. Ferrer, F. Yubero, J. A. Mejia, F. J.- García-Lopez, and A. R. González-Elipe, J. Appl. Phys. **102,** 084112 (2007).
22. G. He, L. D. Zhang, G. H. Li, M. Liu, and X. J. Wang, J. Phys. D: Appl. Phys. **41,** 045304 (2008).
23. D. A. G. Bruggeman, Ann. Phys. **24**, 636 (1935); D. E. Aspnes, Am. J. Phys. **50,** 704 (1982).
24. A. Borras, A. Yanguas-gil, A. Barrance, J. cotino, and A. r. González-Elipe, Phys. Rev. **B 76,** 235303 (2007).
25. D. Mergel, Thin Solid Films **397,** 216 (2001).
26. W. Fawcett, Proc. Phys. Soc. **82,** 33 (1963).
27. V. V. Hoang, Phys. Status Solidi B **244,** 1280 (2007).
28. V. V. Hoang, H. Zung, and N. H. B. Trong, Eur. Phys. J. D **44,** 515 (2007).
29. A. B. Murphy, P. R. F. Barnes, L. K. Randeniya, I. C. Plumb, I. E. Grey, M. D. Horne, and J. A. Glasscock, Int. J. Hydrogen Energ. **31,** 1999 (2006).
30. J.-K. Yao, H.-Y. Li, Z.-X. Fan, Y.-X. Tang, Y.-X. Jin, Y.-A. Zhao, H.-b. He, and J.-D. Shao, Chin. Phys. Lett. **24,** 1964 (2007).
31. J. Yao, C. Xu, J. Ma, M. Fang, Z. Fan, Y. Jin, Yuanan Zhao, H. He, and J. Shao, Appl. Surf. Sci. **255,** 4733 (2009).